Communications on Pure and Applied Analysis
Vol. 21, No. 7, July 2022, pp. 2327–2336
doi:10.3934/cpaa.2022035

ON THE SPHERICAL GEOPOTENTIAL APPROXIMATION FOR SATURN

Susanna V. Haziot

Department of Mathematics, Brown University
Box 1917, Providence, RI 02912, USA

Abstract. In this paper, we show by means of a diffeomorphism that when approximating the planet Saturn by a sphere, the errors associated with the spherical geopotential approximation are so significant that this approach is rendered unsuitable for any rigorous mathematical analysis.

1. **Introduction.** With an equatorial diameter of 120 340km, Saturn is the second largest planet in our solar system, and is located in the sixth position away from the Sun. It is the farthest planet from Earth to have been observed in ancient times and was first seen via telescope in 1610 by Galileo Galilei. Due to the low resolution of his instrument, Galileo mistook the beautiful and complex set of rings revolving around the planet for "handles"; see [10, 7] and the references therein.

Saturn has a volume of about $82\,713\times10^{10}\text{km}^3$ and a mass of about $5.69\times10^{26}\text{kg}$. Whereas its volume is about 60% of Jupiter's, its mass is only about one third of that of its giant neighbor. This is mostly due to the fact that Saturn's rocky core, albeit almost the size of Earth with an equatorial radius of about 5690km, is much smaller than that of Jupiter and that its gaseous envelope of hydrogen and helium is much less compressed. In fact, with a bulk composition of mostly hydrogen, Saturn has a density of about 0.690g/cm^3, meaning that it would float were there a body of water large enough to carry it; see [7].

Since the planet has no solid surface on which a spacecraft could land, collection of data is difficult. In addition, its surface area is of two orders of magnitude greater than that of Earth, making it impossible to observe the entire planet at once at sufficient spatial resolutions for the gathering of useful information. Most notably, the Cassini Orbiter reached the saturnian system on July 1st, 2004. The space probe sent back a wealth of data on Saturn's rings, numerous moons, and finally on its atmosphere, in which, as planned, it disintegrated shortly after entry. Although Saturn itself is not habitable for mankind, the Cassini expedition revealed that some of its moons, such as Titan [15, 16] and Enceladus [1], appear to have Earth-like structures with the possibility of being able to support life. This consequently renders more detailed studies on Saturn as important as well.

2020 *Mathematics Subject Classification.* Primary: 86-10.
Key words and phrases. Atmospheric flow, spherical geopotential approximation.
The author is supported by NSF grant DMS-2102961.

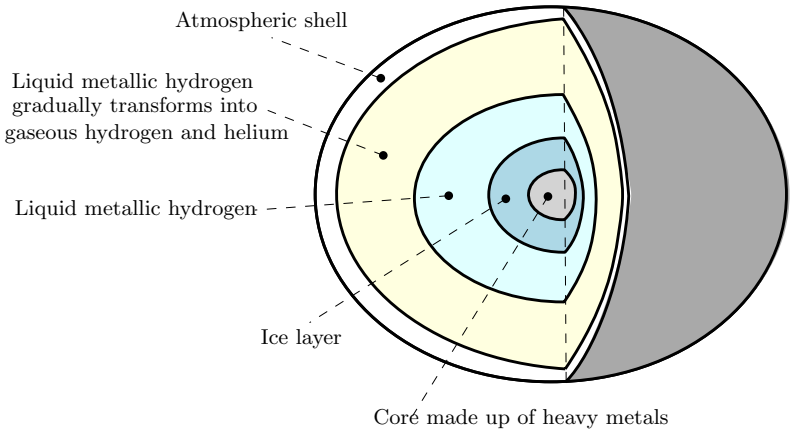

FIGURE 1. A cross section of Saturn depicting the composition of its interior.

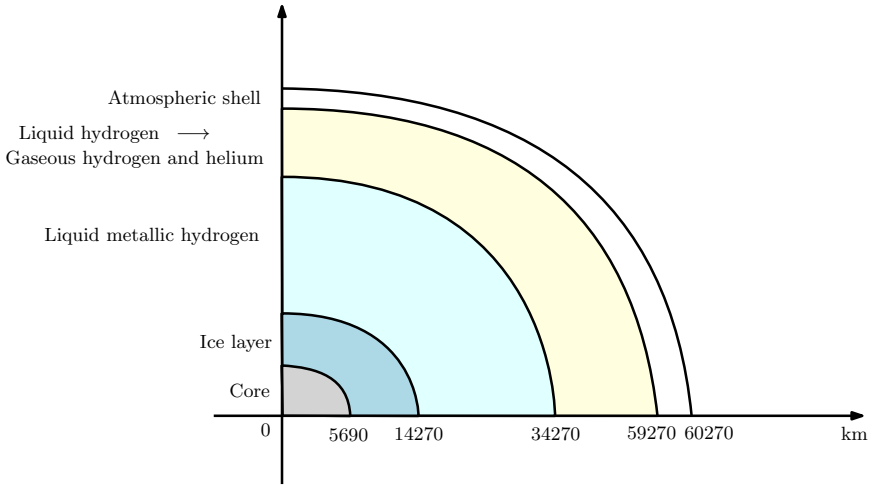

FIGURE 2. The approximate dimensions, in kilometers, of Saturn's layers, measured along the equator; see [14].

Saturn's internal structure has been deduced from studying its gravitational field; see Figures 1 and 2 for a sketch. At the very center lies a solid core, made of heavy metals including metallic iron and molten rock, which is surrounded by water, methane and ammonia. Although this envelop is commonly referred to as "ice layer", it is strongly suspected that the water in it is actually in liquid form. Due to the tremendous pressure in the deep interior, for a span of approximately 20 000km, the hydrogen around the "ices" is maintained in a fluid, metallic state. This layer also contains liquid "helium rains". Within the next 26000km, as the atmospheric pressure exponentially decreases with height, this metallic liquid gradually transforms into a gaseous state consisting of molecular hydrogen and atomic helium. Finally, the atmospheric shell is approximately 1000km wide, starting with a thick and complex layer of stratified clouds in the troposphere of the planet; see[14, 12, 8]. This layer is what gives Saturn its overall hazy and yellow-brown appearance.

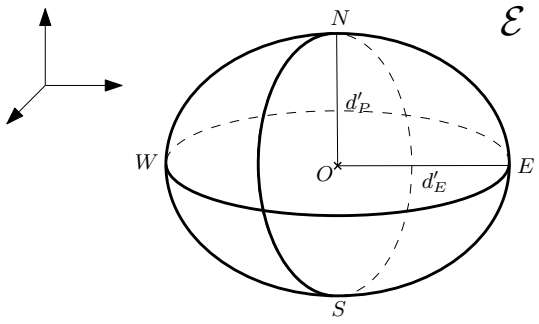

FIGURE 3. Saturn is approximated by an ellispoid $\mathcal{E}$, with polar radius d'_P and equatorial radius d'_E. The polar radius is equal to only about 90.2% of the equatorial one. In comparison, for Earth the polar radius is 99.67% of the equatorial one.

The chemical composition of Saturn's the atmosphere is hydrogen (97%), helium (3%), methane (0.2%) and ammonia (0,03%); see [13]. Atmospheric circulation takes place in zonal flows from east to west, and consists of very strong winds. These create light-colored zones and dark belts. In the equatorial zone, these winds could reach speeds of up to 500m.s^{-1}.

Due to Saturn's gassy composition and rapid rotation (of approximately 10.23hours per rotation), the planet's shape is deformed into an oblate spheroid with flattening at the poles; see [7]. Indeed, it is the least spherical planet in our solar system, with an equatorial diameter that is almost 10% larger than its polar one. More precisely, the equatorial and polar radius are given by

$$d'_E = 60\,269 \text{ km} \qquad \text{and} \qquad d'_P = 54\,364 \text{ km}, \tag{1.1}$$

respectively. Here and for the rest of the paper, the primes denote dimensional quantities and will be removed after non-dimensionalising. As a result of (1.1), the shape of Saturn is roughly that of a ellipsoid; see Figure 3. The aim of this paper is to show that approximating Saturn by a sphere in order to mathematically study its atmospheric shell leads to wildly untrustworthy results unless one looks at the local behavior of atmospheric flows. We will do so by using similar ideas to the ones in [4]. We remark that for limited regions, a spherical approximation is reasonable and one can adapt the developments in [4] for steady flow and in [5] for waves to this context. In particular, this applies to polar vortices in the upper troposphere of Saturn (see the discussion in [6]).

As mentioned above, contrary to Earth, Saturn has no solid ground. In our analysis, we will consider the *ground level* to be situated right below the atmospheric shell, that is, the point at which all liquid hydrogen has been transformed into gas. The atmospheric shell we consider spans 1000km along the equator; see Figure 2 for a sketch depicting the approximate width along the equator of each layer of Saturn's interior; see also [14, 12].

The plan of the paper is the following: we begin by describing how to approximate Saturn by an ellipsoid, thus taking into account the oblateness of the planet. We then show by means of a diffeomorphism that the distortion errors in approximating Saturn by a sphere are of the order of 60%, rendering any large-scale result obtained in such a way unreliable.

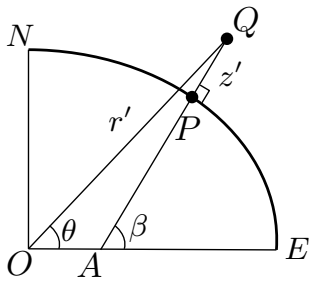

FIGURE 4. The spherical and geopotential coordinate systems for fixed longitude φ. Here θ denotes the geocentric latitude of the point Q. The normal vector of the ellipsoid $\mathcal{E}$ at Q intersects the equatorial plane at the focus point A, at an angle β, called the geodetic latitude angle of P.

2. **Ellipsoidal approximation.** As mentioned in the introduction, we approximate Saturn by an ellipsoid which we will denote by $\mathcal{E}$. Specifically, we consider an ellipse whose center coincides with that of Saturn. We set the semi-major axis to be equal to Saturn's equatorial radius d'_E and the semi-minor axis to the polar radius d'_P. The values of these quantities are provided in (1.1). We now equip the ellipsoid $\mathcal{E}$ obtained by rotating this ellipse about the semi-minor axis, with the Cartesian coordinates (X', Y', Z') such that the origin coincides with Saturn's center O; see Figure 3.

Any point Q in Saturn's atmospheric shell can be expressed in terms of the spherical coordinates (φ, θ, r'). Here $r' = |OQ|$ denotes the distance between Q and the center of Saturn, $\varphi \in [0, 2\pi)$ the eastward angle of longitude and $\theta \in \left[-\frac{\pi}{2}, \frac{\pi}{2}\right]$ the geocentric angle; see Figure 4.

Let us now consider the normal to the ellipsoid $\mathcal{E}$ through Q, which intersects $\mathcal{E}$ at the point P and the equatorial plane at the point A. Then Q can also be expressed in terms of the geopotential coordinates (φ, β, z'). Here, $z' = |PQ|$ is the height of Q above Saturn's ground level and $\beta \in \left[-\frac{\pi}{2}, \frac{\pi}{2}\right]$ denotes the geodetic, or geographic, latitude of Q; see Figure 4. The unit tangent vectors in the system, at the surface of the ellipsoid are $(\mathbf{e}_\varphi, \mathbf{e}_\beta, \mathbf{e}_z)$. Note that this system is valid throughout the space, with the exception of along the direction of the polar axis, since $\mathbf{e}_\varphi$ and $\mathbf{e}_\beta$ aren't well-defined at the two poles.

Finally, one can go from the Cartesian coordinate system to the geopotential one with the following transformation:

$$(X', Y', Z') = \frac{d'_E}{\sqrt{1 - \mathfrak{e}^2 \sin^2 \beta}} (\cos\beta \cos\varphi, \cos\beta \sin\varphi, (1 - \mathfrak{e}^2) \sin\beta).$$

Here, $\mathfrak{e}$ denotes the eccentricity of the geoid and is given by

$$\mathfrak{e} = \sqrt{1 - \left(\frac{d'_P}{d'_E}\right)^2} \approx 0.43.$$

The Cartesian coordinates of the ellipsoid $\mathcal{E}$ can also be expressed in terms of the geocentric latitude α by

$$(X', Y', Z') = d'(\cos\alpha \cos\varphi, \cos\alpha \sin\varphi \sin\alpha).$$

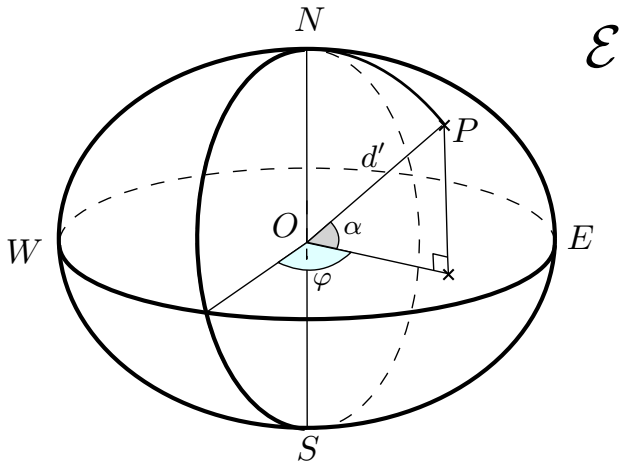

FIGURE 5. Saturn viewed as an ellipsoid with a point P on its surface expressed in terms of the geocentric latitude α. The angle α is related to the geodetic latitude β by (2.1).

Here

$$d' = \frac{d'_P}{\sqrt{1-\mathfrak{e}^2\cos^2\alpha}} = d'_E\sqrt{\frac{1-\mathfrak{e}^2(2-\mathfrak{e}^2)\sin^2\beta}{1-\mathfrak{e}^2\sin^2\beta}}$$

is the distance from a point on $\mathcal{E}$ to the center of Saturn O, so that in the Northern Hemisphere we have

$$\alpha = \arctan\big((1-\mathfrak{e}^2)\tan\beta\big); \tag{2.1}$$

see Figure 5.

This ellipsoidal approximation now accommodates for the oblateness of Saturn. This can then be used to transform any set of governing equations (such as for example Navier-Stokes) expressed in spherical coordinates to take into account the vertical height of the ellipsoid. This has been done by Constantin and Johnson to derive a system of equations governing the dynamics of the atmosphere of Earth; see [4].

A natural question would be whether one could approximate Saturn by a sphere when studying, for instance, its atmosphere. Indeed, this is typically what is done for sphere-like elements by means of what is referred to as the *spherical geopotential approximation*. For the remainder of the paper, following the ideas in [4], we show that the perturbation of spherical coordinates is an invalid choice of coordinate system when studying a planet as oblate as Saturn. Indeed, we prove that the errors involved preclude any reliable analytical results of large-scale atmospheric flows.

3. **Spherical geopotential approximation.**

The spherical geopotential approximation consists of approximating the geoid by a spherical surface (see for instance [2] and [17]). We remark the importance of the relevance of inviscid flow for the stratosphere and the fact that the rapid rotation of Saturn ensures that the large-scale atmospheric flow is geostrophically balanced. As a result, in the horizontal momentum equations the dominant force balance is between pressure gradient and Coriolis forces (see the discussion [9]).

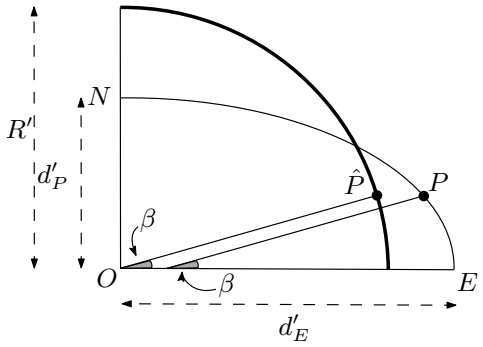

FIGURE 6. The spherical geopotential approximation for fixed longitude φ. The point P on the ellipsoid is mapped into $\hat{P}$ on the sphere of radius R'. This is obtained by setting the geocentric latitude angle of $\hat{P}$ to be equal to the geodetic latitude of P.

To carry out the spherical geophysical approximation, we choose a sphere of radius of R', where

$$R' = \sqrt{\frac{d_E'^2 + d_P'^2}{2}}.$$

The longitude on this sphere is simply the longitude φ on the ellipsoid $\mathcal{E}$. However, the value of the latitude on the sphere will be the geodetic latitude β on $\mathcal{E}$; see Figure 6. This approximation is, for instance, used for Earth in most meterological global models as well as in operational meterological forcast systems. As can be seen in Figure 6, when the ellipsoid we are approximating is very close to being a sphere, the location of the point P on the ellipsoid very closely coincides with its corresponding point $\hat{P}$ on the sphere. However, the greater the oblateness of the geoid, the further the point we study on the sphere is from the point we actually wish to investigate on the ellipsoid. We will see in the next section how big this error can get in the case of Saturn.

Let us now consider a point Q in Saturn's atmospheric shell. We assume that the point $P(\varphi, \beta)$ is the orthogonal projection of Q onto the *ground level* (as defined in the introduction) of the planet. We denote the vertical distance between P and Q by z_e'. The spherical geopotential approximation then maps Q to the point $\hat{Q}$ with geocentric spherical coordinates $(\varphi, \alpha, R' + z_e')$. Recall the relationship between α and β, as provided in (2.1).

More specifically, since the outward unit normal vector to the geoid at the point P is given by

$$(\cos\beta\cos\varphi, \cos\beta\sin\varphi, \sin\beta).$$

the underlying transformation maps the point Q, with coordinates

$$Q = \left[\frac{d_E'}{\sqrt{1-\mathfrak{e}^2\sin^2\beta}} + z_e'\right]\left(\cos\beta\cos\varphi, \cos\beta\sin\varphi, (1-\mathfrak{e}^2)\sin\beta\right) + (0, 0, z_e'\mathfrak{e}^2\sin\beta)$$

to the point $\hat{Q}$, given by

$$\hat{Q} = (R' + z_e')(\cos\beta\cos\varphi, \cos\beta\sin\varphi, \sin\beta).$$

In order to appreciate how the spherical geopotential approximation distorts distances in Saturn's atmospheric shell we non-dimensionalize the problem using a

length scale of 1km. Any point in this shell is situated within 1000km of the ground level. From this point on, we will drop all the primes to denote dimensionless quantites.

Let us now denote by $\mathcal{O}_e$ the open region between the ellipsoid $\mathcal{E}$ and a parallel ellipsoid at a distance of 1000, with the two segments along the polar axis excised. Moreover, we define $\mathcal{O}_s$ to be the open region, centered at the origin, between the sphere of radius R and that of radius $R + 1000$. Here once again, we remove all points along the polar axis.

The idea is now to study the smooth diffeomorphism $\mathscr{F}$ that maps the point

$$\left[\frac{d_E}{\sqrt{1-\mathfrak{e}^2\sin^2\beta}} + z_e\right]\left(\cos\beta\cos\varphi, \cos\beta\sin\varphi, (1-\mathfrak{e}^2)\sin\beta\right) + (0, 0, z_e\mathfrak{e}^2\sin\beta)$$

in $\mathcal{O}_e$ to the point

$$(R + z_e)(\cos\beta\cos\varphi, \cos\beta\sin\varphi, \sin\beta)$$

in the spherical shell $\mathcal{O}_s$.

We first establish that $\mathscr{F}$ is a continuous bijection from $\mathcal{O}_e$ onto $\mathcal{O}_s$. Before we do so, note that since the ellipsoid $\mathcal{E}$ is a closed convex set in $\mathbb{R}^3$, for any point $x \in \mathbb{R}^3$ we can find a unique point $x_e \in \mathcal{E}$ closest to it. Indeed, since $\mathcal{E}$ is closed, existence is guaranteed. Moreover, uniqueness can easily be shown with an argument by contradiction involving the convexity of $\mathcal{E}$; see [11] for details. The map $m : x \to x_e$ is called the metric projection of $\mathbb{R}^3$ onto $\mathcal{E}$ with respect to the Euclidean norm. By a result due to Busemann and Feller [3] (see also [11]), this metric projection is hence non-expansive.

Now, since by (2.1) we have an explicit, bijective relationship between the geodetic latitude β and the geocentric latitude α of a point on $\mathcal{E}$, $\mathscr{F}$ clearly is a continuous bijection from $\mathcal{O}_e$ onto $\mathcal{O}_s$.

We must now check that the map $\mathscr{F}$ is indeed a diffeomorphism between $\mathcal{O}_e$ and $\mathcal{O}_s$. To this end, we first consider the transformation $\mathscr{F}_1$, which maps the spherical coordinates $(\varphi, \beta, R + z_e)$ to the point

$$\left[\frac{d_E}{\sqrt{1-\mathfrak{e}^2\sin^2\beta}} + z_e\right]\left(\cos\beta\cos\varphi, \cos\beta\sin\varphi, (1-\mathfrak{e}^2)\sin\beta\right) + (0, 0, z_e\mathfrak{e}^2\sin\beta).$$

Specifically, the Jacobian J_1 of this transformation can be calculated to be

$$J_1 = \begin{pmatrix} -M\cos\beta\sin\varphi & M\cos\beta\cos\varphi & 0 \\ -N\sin\beta\cos\varphi & -N\sin\beta\sin\varphi & N\cos\beta \\ \cos\beta\cos\varphi & \cos\beta\sin\varphi & \sin\beta \end{pmatrix},$$

where M and N are given by

$$M := \left[\frac{d_E}{\sqrt{1-\mathfrak{e}^2\sin^2\beta}} + z_e\right] \qquad \text{and} \qquad N := \left[\frac{d_E(1-\mathfrak{e}^2)}{(1-\mathfrak{e}^2\sin^2\beta)^{3/2}} + z_e\right],$$

respectively. In particular, J_1 has a non-singular determinant away from the polar axis $\beta = \pm\frac{\pi}{2}$. Indeed, we can calculate that

$$\det(J_1) = \left(\frac{d_E}{\sqrt{1-\mathfrak{e}^2\sin^2\beta}} + z_e\right)\left(\frac{d_E(1-\mathfrak{e}^2)}{(1-\mathfrak{e}^2\sin^2\beta)^{3/2}} + z_e\right)\sin\beta \neq 0.$$

We now introduce the transformation $\mathscr{F}_2$, which maps the spherical coordinates $(\varphi, \beta, R + z_e)$ to the point

$$(R + z_e)(\cos\beta\cos\varphi, \cos\beta\sin\varphi, \sin\beta).$$

Here, we find the corresponding Jacobian J_2 to be

$$J_2 = \begin{pmatrix} -(R+z_e)\cos\beta\sin\varphi & (R+z_e)\cos\beta\cos\varphi & 0 \\ -(R+z_e)\sin\beta\cos\varphi & -(R+z_e)\sin\beta\sin\varphi & (R+z_e)\cos\beta \\ \cos\beta\cos\varphi & \cos\beta\sin\varphi & \sin\beta \end{pmatrix}.$$

We are now ready to consider the map

$$\mathscr{F} = \mathscr{F}_2 \circ \mathscr{F}_1^{-1}.$$

Specifically, we deduce that the Jacobian J of this transformation is given by

$$J = J_2 J_1^{-1} = \begin{pmatrix} \frac{(R+z_e)\sqrt{1-\mathfrak{e}^2\sin^2\beta}}{d_E + z_e\sqrt{1-\mathfrak{e}^2\sin^2\beta}} & 0 & 0 \\ 0 & \frac{(R+z_e)^2(1-\mathfrak{e}^2\sin^2\beta)^3}{\left[d_E(1-\mathfrak{e}^2)+z_e(1-\mathfrak{e}^2\sin^2\beta)^{3/2}\right]^2} & 0 \\ 0 & 0 & 1 \end{pmatrix}.$$

Notice that the determinant of J does not vanish in $\mathcal{O}_e$. Therefore, by the inverse function theorem, $\mathscr{F}$ is a smooth local diffeomorphism. Combining this with the fact that $\mathscr{F}$ is a continuous bijection between $\mathcal{O}_e$ and $\mathcal{O}_s$ yields that it is a diffeomorphism between $\mathcal{O}_e$ and $\mathcal{O}_s$.

4. **Distortion errors.** In order to understand the errors associated with spherical geopotential approximation, we compute the metric tensor of $\mathscr{F}$. This is given by

$$\begin{pmatrix} \frac{(R+z_e)^2(1-\mathfrak{e}^2\sin^2\beta)}{[d_E+z_e\sqrt{1-\mathfrak{e}^2\sin^2\beta}]^2} & 0 & 0 \\ 0 & \frac{(R+z_e)^2(1-\mathfrak{e}^2\sin^2\beta)^3}{[d_E(1-\mathfrak{e}^2)+z_e(1-\mathfrak{e}^2\sin^2\beta)^{3/2}]^2} & 0 \\ 0 & 0 & 1 \end{pmatrix}. \tag{4.1}$$

The orthogonality of the spherical geopotential approximation is reflected by the fact that this tensor is diagonal. Moreover, were the metric tensor equal to the identity matrix, we would have no distortion errors associated with this transformation. It is interesting to note that the first two terms in the diagonal of (4.1) differ from the value 1 only by an order of at most $\mathfrak{e}^2$. For sufficiently small $\mathfrak{e}$, this suggests that distorting the geometry from ellipsoidal to spherical may yield valid results up to leading order approximations.

In order to get a more precise assessment of the errors involved, we further examine the metric tensor, and specifically, find bounds for the first two terms in the diagonal of (4.1). Recall that $d_E > R$. Moreover, we have

$$1 - \mathfrak{e}^2 \le 1 - \mathfrak{e}^2\sin^2\beta \le 1, \tag{4.2}$$

by simply setting $\sin^2\beta = 0$ and $\sin^2\beta = 1$ in the middle term. Denoting by

$$s(\beta) := \sqrt{1 - \mathfrak{e}^2\sin^2\beta},$$

we define the function

$$f(s) : s \mapsto \frac{s}{d_E + z_e s},$$

for fixed $z_e \ge 0$. We can easily check that

$$f'(s) = \frac{d_E}{(d_E + z_e s)^2} \ge 0, \qquad \text{since} \quad d_E \ge 0.$$

Hence we see that the function f is increasing in s. Combining this with (4.2), we find the following upper and lower bounds

$$\frac{(R+z_e)^2(1-\mathfrak{e}^2)}{[d_E+z_e\sqrt{1-\mathfrak{e}^2}]^2} \leq \frac{(R+z_e)^2(1-\mathfrak{e}^2\sin^2\beta)}{[d_E+z_e\sqrt{1-\mathfrak{e}^2\sin^2\beta}]^2} \leq \frac{(R+z_e)^2}{[d_E+z_e]^2} < 1 \tag{4.3}$$

for the first term in the diagonal of (4.1). Following the same approach for the second term, we obtain the following bounds:

$$\frac{(R+z_e)^2(1-\mathfrak{e}^2)}{[d_E+z_e\sqrt{1-\mathfrak{e}^2}]^2} \leq \frac{(R+z_e)^2(1-\mathfrak{e}^2\sin^2\beta)^3}{[d_E(1-\mathfrak{e}^2)+z_e(1-\mathfrak{e}^2\sin^2\beta)^{3/2}]^2} \leq \frac{(R+z_e)^2}{[d_E(1-\mathfrak{e})+z_e]^2}. \tag{4.4}$$

It is straight-forward to check that

$$\frac{d_E}{\sqrt{1-\mathfrak{e}^2}} > R > d_E(1-\mathfrak{e}^2) \tag{4.5}$$

holds. In addition, from (4.3) we see that

$$0 < 1 - \frac{(R+z_e)^2(1-\mathfrak{e}^2)}{[d_E+z_e\sqrt{1-\mathfrak{e}^2}]^2} = 1 - \frac{(R+z_e)^2}{\left(\frac{d_E}{\sqrt{1-\mathfrak{e}^2}}+z_e\right)^2}, \tag{4.6}$$

where the equality results from a simple reformulation. By taking a derivative with respect to z_e and by using (4.5), we see that the map

$$z_e \mapsto \frac{(R+z_e)^2}{\left(\frac{d_E}{\sqrt{1-\mathfrak{e}^2}}+z_e\right)^2}$$

is strictly increasing. Combining this with (4.6), we find the following upper bound for $z_e = 0$:

$$0 < 1 - \frac{(R+z_e)^2}{\left(\frac{d_E}{\sqrt{1-\mathfrak{e}^2}}+z_e\right)^2} \leq 1 - \frac{R^2}{\left(\frac{d_E}{\sqrt{1-\mathfrak{e}^2}}\right)^2} = \frac{3}{2}\mathfrak{e}^2 - \frac{1}{2}\mathfrak{e}^4 \tag{4.7}$$

We now turn to (4.4) and see that

$$0 < \frac{(R+z_e)^2}{[d_E(1-\mathfrak{e}^2)+z_e]^2} - 1.$$

Using (4.5) once more, and as above, taking a derivative with respect to z_e, we see that the map

$$z_e \mapsto \frac{(R+z_e)^2}{[d_E(1-\mathfrak{e}^2)+z_e]^2}$$

is strictly decreasing, and therefore, for $z_e = 0$, we get

$$0 < \frac{(R+z_e)^2}{[d_E(1-\mathfrak{e}^2)+z_e]^2} - 1 \leq \frac{R^2}{d_E^2(1-\mathfrak{e}^2)^2} - 1 = \frac{\frac{3}{2}\mathfrak{e}^2-\mathfrak{e}^4}{(1-\mathfrak{e}^2)^2}. \tag{4.8}$$

By comparing (4.7) and (4.8), we see that the maximum value of these bounds is given by

$$\frac{\frac{3}{2}\mathfrak{e}^2-\mathfrak{e}^4}{(1-\mathfrak{e}^2)^2} \approx 0.366,$$

and is attained at the equatorial ground level, when $z_e = \beta = 0$. As a result, the errors in identifying the position of points in Saturn's atmospheric shell are given, in non-dimensional terms, by $\sqrt{0.366}$. This is equivalent to an error of roughly 60% in the meridional direction around the sphere.

Acknowledgements. The author is grateful to the referees for their helpful suggestions.

REFERENCES

[1] A. Affholder, F. Guyot, B. Sauterey, R. Ferrière and S. Mazevet, Bayesian analysis of Enceladus's plume data to assess methanogenesis, *Nat. Astron.*, **8** (2021), 805–814.
[2] P. Benard, An oblate-spheroid geopotential approximation for global meteorology, *Quart. J. Roy. Meterol. Soc.*, **140** (2014), 170–184.
[3] H. Busemann and W. Feller, Krümmungseigenschaften konvexer Flächen, *Acta Math.*, **66** (1936), 1–47.
[4] A. Constantin and R. S. Johnson, On the modelling of large-scale atmospheric flow, *J. Differ. Equ.*, **285** (2021), 751–798.
[5] A. Constantin and R. S. Johnson, On the propagation of waves in the atmosphere, *Proc. A*, **477** (2021), 25 pp.
[6] A. Constantin, D. G. Crowdy, V. S. Krishnamurthy and M. H. Wheeler, Stuart-type polar vortices on a rotating sphere, *Discrete Cont. Dyn. Syst.*, **41** (2021), 201–215.
[7] G. Faure and T. M. Mensing, *Introduction to Planetary Science: The Geological Perspective*, Springer, Dordrecht, The Netherlands, 2007.
[8] R. A. Freedman and W. J. Kaufmann III, *Universe:The Solar System*, Freeman, New York, NY, 2002.
[9] B. Galperin and P.L. Read, *Zonal Jets: Phenomenology, Genesis and Physics*, Cambridge University Press, Cambridge, 2019.
[10] E. Gregersen, *The Outer Solar System*, Britannica Educational Publishing, New York, NY, 2009.
[11] P. Gruber, *Convex and Discrete Geometry*, Springer-Verlag, Berlin-Heidelberg, 2007.
[12] W. K. Hartmann, *Moons and Planets*, Brooks/Cole, Belmont, CA, 2005.
[13] A. P. Ingersoll, et al., *Atmospheres of the giant planets* in *The New Solar System*, Sky Publishing, Cambridge, MA, 1999.
[14] J. E. Klepeis, et al., Hydrogen-helium mixtures at megabars pressure: Implications for Jupiter and Saturn, *Science*, **254** (1991), 986–989.
[15] J. Lunine, Saturn's Titan: A Strict Test for Life's Cosmic Ubiquity, *Proceed. Amer. Phil. Soc.*, **153** (2009), 403–418.
[16] NASA/Jet Propulsion Laboratory, Life on Titan? New clues to what's consuming hydrogen, acetylene on Saturn's moon, *Sci. Daily*, 2010.
[17] A. Staniforth, Spherical and spheroidal geopotential approximations, *Quart. J. Roy. Meterol. Soc.*, **140** (2014), 2685–2692.

Received October 2021; revised December 2021; early access February 2022.

E-mail address: susanna_haziot@brown.edu